

A near-global climatology of oceanic coherent eddies

Josué Martínez-Moreno¹, Andrew McC. Hogg¹, and Matthew H. England²

¹Australian National University

²University of New South Wales

November 22, 2022

Abstract

Ocean eddies influence regional and global climate through mixing and transport of heat and properties. One of the most recognizable and ubiquitous feature of oceanic eddies are coherent vortices with spatial scales of tens to hundreds of kilometers, frequently referred as “mesoscale eddies”. Coherent mesoscale eddies are known to transport properties across the ocean and to locally affect near-surface wind, cloud properties, and rainfall patterns. Although coherent eddies are ubiquitous, their climatology, seasonality, and long-term temporal evolution remains poorly understood. Here, we examine the kinetic energy contained by coherent eddies and present the seasonal, interannual and long-term variability using satellite observations between 1993 to 2019. A total of ~ 37 million coherent eddies are detected in this analysis. Around 50% of the kinetic energy contained by ocean eddies corresponds to coherent eddies. Additionally, a strong seasonal cycle is observed, with a 3-6 months lag between the wind forcing and the response of the coherent eddy field. The seasonality of the number of coherent eddies and their amplitude reveals that the number of coherent eddies responds faster to the forcing (~ 3 months), than the coherent eddy amplitude (which lags by ~ 6 months). This seasonal cycle is spatially variable, so we also analyze their climatology in key oceanic regions. Our analysis highlights the relative importance of the coherent eddy field in the ocean kinetic energy budget, implies a strong response of the eddy number and eddy amplitude to forcing at different time-scales, and showcases the seasonality, and multidecadal trends of coherent eddy properties.

A near-global climatology of oceanic coherent eddies

Josué Martínez-Moreno¹, Andrew McC. Hogg¹, and Matthew H. England²

¹Research School of Earth Science and ARC Center of Excellence for Climate Extremes, Australian National University, Canberra, Australia

²Climate Change Research Centre (CCRC), UNSW Australia, Sydney NSW, Australia

Key Points:

- Coherent eddies contain around 50% of the total surface ocean kinetic energy budget.
- Seasonal cycle of the number of coherent eddies and the coherent eddy amplitude reveals a 3-6 month lag to wind forcing.
- The seasonal lag between the number and the amplitude of coherent eddies suggests a role for the inverse cascade.

Corresponding author: Josué Martínez-Moreno, josue.martinezmoreno@anu.edu.au

Abstract

Ocean eddies influence regional and global climate through mixing and transport of heat and properties. One of the most recognizable and ubiquitous feature of oceanic eddies are coherent vortices with spatial scales of tens to hundreds of kilometers, frequently referred as “mesoscale eddies”. Coherent mesoscale eddies are known to transport properties across the ocean and to locally affect near-surface wind, cloud properties, and rainfall patterns. Although coherent eddies are ubiquitous, their climatology, seasonality, and long-term temporal evolution remains poorly understood. Here, we examine the kinetic energy contained by coherent eddies and present the seasonal, interannual and long-term variability using satellite observations between 1993 to 2019. A total of ~ 37 million coherent eddies are detected in this analysis. Around 50% of the kinetic energy contained by ocean eddies corresponds to coherent eddies. Additionally, a strong seasonal cycle is observed, with a 3–6 months lag between the wind forcing and the response of the coherent eddy field. The seasonality of the number of coherent eddies and their amplitude reveals that the number of coherent eddies responds faster to the forcing (~ 3 months), than the coherent eddy amplitude (which lags by ~ 6 months). This seasonal cycle is spatially variable, so we also analyze their climatology in key oceanic regions. Our analysis highlights the relative importance of the coherent eddy field in the ocean kinetic energy budget, implies a strong response of the eddy number and eddy amplitude to forcing at different time-scales, and showcases the seasonality, and multidecadal trends of coherent eddy properties.

Plain language summary

Coherent eddies are the most common feature of ocean variability observable from satellites. They are crucial in ocean dynamics as they can transport properties over long distances and interact with the atmosphere. Our study investigates the seasonal, interannual, and long-term changes in the abundance and intensity of coherent eddies, by automatically identifying individual eddies over the available satellite altimeter record. The seasonal cycle suggests a transition from numerous, smaller, and weaker coherent eddies, to fewer and larger, and stronger coherent eddies over the season. In addition, a long-term adjustment of the coherent eddy field is identified with possible links to long-term changes in the climate system.

1 Introduction

Mesoscale ocean variability with spatial scales of tens to hundreds of kilometers is comprised of processes such as vortices, waves, and jets (Ferrari & Wunsch, 2009; Fu et al., 2010). These mesoscale processes are highly energetic, and they play a crucial role in the transport of heat, salt, momentum, and other tracers through the ocean (Wunsch & Ferrari, 2004; Wyrski et al., 1976; Gill et al., 1974). One of the most recognizable and abundant ocean processes observable from space are mesoscale vortices. Although mesoscale vortices are commonly referred to in the literature as “mesoscale eddies”, this term is also often used to describe the total mesoscale ocean variability (the time-varying component of the mesoscale flow), thus, to avoid ambiguity we will refer to mesoscale vortices as *coherent eddies*. Coherent eddies are abundant and energetic; they are essential to ocean dynamics as concluded by many previous studies (Hogg & Blundell, 2006; Siegel et al., 2011; Beron-Vera et al., 2013; Frenger et al., 2013, 2015; Pilo et al., 2015; Schubert et al., 2019; Patel et al., 2020).

Coherent eddies are quasi-circular geostrophic currents. According to their rotational direction and the sign of the Coriolis parameter, the sea surface height anomaly within a coherent eddy can have a negative or positive sea surface height anomaly (cold-core and warm-core coherent eddies, respectively). This characteristic sea surface height signature of coherent eddies has been utilized to identify and track coherent eddies from satellite altimetry (e.g., Chelton et al., 2007; Faghmous et al., 2015; Ashkezari et al., 2016; Martínez-Moreno et al., 2019; Cui et al., 2020). Automated identification algorithms of coherent eddies have revealed their ubiquity in the oceans, with a predominant influence at hotspots of eddy activity such as in boundary current extensions and the Antarctic Circumpolar Current. In these regions, it has been estimated that coherent eddies contribute around 40–50% of the net mesoscale kinetic energy (Chelton et al., 2011) and thus a significant fraction of the total kinetic energy (Ferrari & Wunsch, 2009). Although this estimate showcases the importance of the mesoscale coherent eddy field, the energy contained by coherent eddies was estimated by extracting the total geostrophic velocity within the radius of each detected coherent eddy; thus, it is possible that this estimate may contain energy from other processes. Here we extend on this past work by reconstructing the surface imprint of coherent eddies using a new eddy tracking algorithm and using the latest available satellite record.

76 There is broad consensus that mesoscale eddy kinetic energy has a pronounced sea-
77 sonal variability (Qiu, 1999; Qiu & Chen, 2004; Kang & Curchitser, 2017; Uchida et al.,
78 2017). Several hypotheses have been proposed to explain this seasonality including: sea-
79 sonal variations of atmospheric forcing (Sasaki et al., 2014), seasonality of the mixed layer
80 depth (Qiu et al., 2014; Callies et al., 2015), seasonality of the intensity of barotropic in-
81 stability (Qiu & Chen, 2004), the variability of the baroclinic instability due to the sea-
82 sonality of the vertical shear (Qiu, 1999), and a seasonal lag of the inverse energy cas-
83 cade (i.e. energy is transported between scales, from small to large; Arbic et al., 2013)
84 in combination with the presence of a front in the mixed layer, which can lead to a sea-
85 sonal cycle of the baroclinic instability (Qiu et al., 2014). On one hand, processes such
86 as barotropic and baroclinic instabilities control the seasonality of coherent eddies in the
87 ocean. On the other hand, recent studies using observations and eddy-permitting climate
88 models suggest slower adjustments of the global ocean that create long-term changes in
89 the coherent eddy field. Such readjustments include a multidecadal increase in the ocean
90 stratification resulting from temperature and salinity changes (Li et al., 2020), a hori-
91 zontal readjustment of sea surface temperature gradients (Cane et al., 1997; Bouali et
92 al., 2017; Ruela et al., 2020), and an intensification of the kinetic energy, eddy kinetic
93 energy, and mesoscale eddy kinetic energy over the last 3 decades as a consequence of
94 an increase in wind forcing (Hu et al., 2020; Wunsch, 2020; Martínez-Moreno et al., 2021).
95 All of these seasonal factors and long-term readjustments directly influence the annual
96 and decadal response of the coherent eddy field, however, the seasonality of the coher-
97 ent component of the eddy kinetic energy, as well as the seasonal cycle and trends of the
98 coherent eddy statistics, remain unknown.

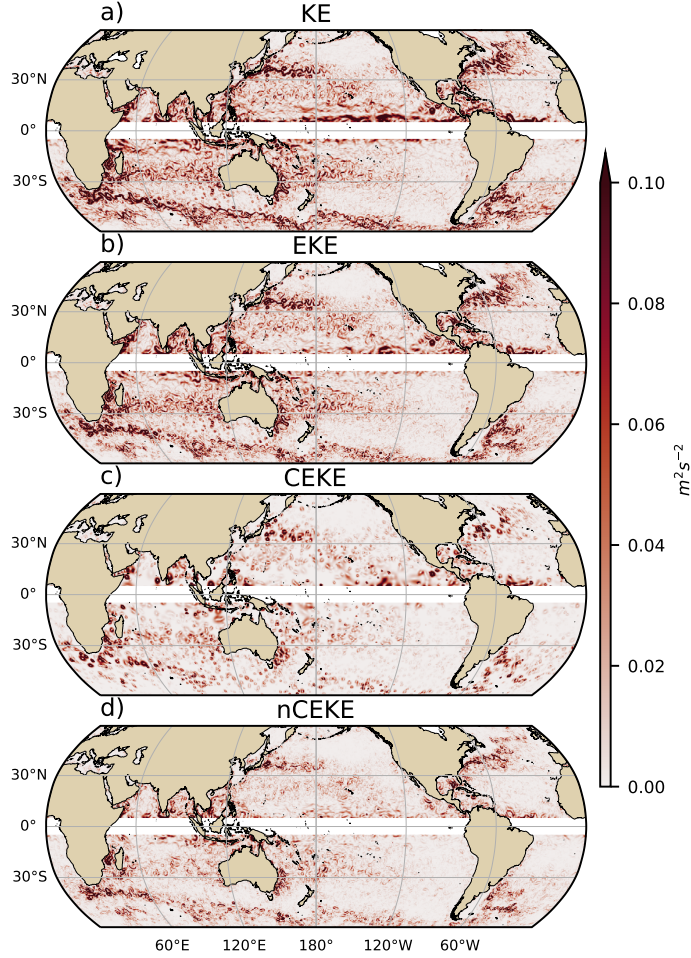
99 Here we present a new global climatology of the coherent eddy kinetic energy by
100 reconstructing the coherent eddy signature from satellite observations. Our study doc-
101 uments the seasonal cycle of the coherent eddy kinetic energy, and the seasonal cycle and
102 long-term trends of the coherent eddy properties over the satellite record. Moreover, we
103 conduct more detailed analyses in regions where coherent eddies dominate the eddy ki-
104 netic energy field. The rest of this paper is structured as follows: the data sources and
105 methodology are described in Section 2. Then, we present the climatology, energy ra-
106 tios, and global seasonality of the coherent eddy kinetic energy in Section 3. Section 4
107 outlines the global climatology and seasonality of coherent eddy properties, followed by
108 long-term changes of the coherent eddy properties (Section 5). Then we focus our at-

109 attention on the seasonal cycle and coherent eddy properties in regions dominated by co-
110 herent eddies (Section 6). Finally, Section 7 summarizes the main results and discusses
111 the implications of this study.

112 2 Methods

113 We use daily sea surface height (SSH) data made available by the Copernicus Ma-
114 rine Environment Monitoring Service in near real time (CMEMS, 2017). This gridded
115 product contains the sea surface height and geostrophic velocities with daily 0.25° res-
116 olution from January 1993 to 2019. The daily geostrophic velocities allow us to compute
117 the kinetic energy (KE) and eddy kinetic energy (EKE) over the satellite record. The
118 main source of EKE is the time-varying wind (Ferrari & Wunsch, 2009); thus, we also
119 compute the seasonal cycle of the wind magnitude from the JRA55 reanalysis (Japan
120 Meteorological Agency, Japan, 2013) using wind velocities at 10m above the ocean's sur-
121 face.

122 Over the same record, coherent eddy statistics from Martínez-Moreno et al. (2019),
123 hereafter MM19, are analyzed and compared with those released by Chelton & Schlax
124 (2013), hereafter CS13. Both datasets are gridded in a 1° resolution and are produced
125 via automated eddy identification algorithms using closed contours of SSH. However, these
126 datasets have important differences in the criteria they use to identify and record coher-
127 ent eddies statistics. The major differences include: (i) MM19's algorithm requires an
128 adjustment between a 2D Gaussian and the SSH anomaly (SSHa) surface within the iden-
129 tified closed contour, while CS13's only uses the outermost closed contour of SSH; (ii)
130 MM19's dataset reports the maximum SSHa within the identified coherent eddy, while
131 CS13's algorithm reports the maximum SSH value minus the discrete level in which the
132 coherent eddy was identified; and (iii) MM19's dataset includes all detected coherent ed-
133 dies, while CS13's dataset excludes coherent eddies with lifetimes shorter than four weeks
134 and coherent eddy amplitudes smaller than 1cm. Moreover, MM19's algorithm allows
135 the reconstruction of the coherent eddy field under the assumption that coherent eddies
136 have a 2D Gaussian imprint in the sea surface height. This Gaussian reconstruction of
137 the coherent eddy field then allows us to estimate the coherent geostrophic eddy veloc-
138 ities and thus the kinetic energy contained only by coherent eddies.



155 **Figure 1.** Snapshot of surface kinetic energy (\overline{KE}), surface eddy kinetic energy (\overline{EKE}),
 156 surface coherent eddy kinetic energy (\overline{CEKE}), and surface non-coherent eddy kinetic energy
 157 (\overline{nCEKE}) for the 1st of January 2017.

167 Note that the $cEddy_{amp}^+$ and $cEddy_{amp}^-$ are sign definite, thus the difference will always
 168 be positive, whereas the gridded averaged $cEddy_{amp}$ can be negative or positive noting
 169 the dominant polarity of coherent eddies in the region, and the absolute value of $cEddy_{amp}$
 170 is denoted by $cEddy_{|amp|}$. We analyze the climatology and trends of the above eddy statis-
 171 tics over the available satellite record, namely between 1993 and 2019. We exclude the
 172 equatorial region ($10^\circ S - 10^\circ N$) and regions poleward of 60° , because the geostrophic ap-
 173 proximation is invalid near the Equator and the satellite spatial coverage at high-latitudes
 174 is unable to resolve the coherent eddy scales polewards of 60° . Note that the climatol-
 175 ogy of $cEddy_n$ is computed by adding all the identified eddies over the record, while all

176 other climatological statistics are computed as the time-average over the record. Sea-
 177 sonal climatologies are calculated for the monthly average of each coherent eddy statis-
 178 tic, while hemispheric time-series are filtered with a running average of 90 days. Trends
 179 of $cEddy_n$ and $|cEddy_{amp}|$ are calculated by coarsening the dataset to a 5° grid, and then
 180 linear trends are computed for each grid point. The statistical significance of trends is
 181 assessed by a modified Mann-Kendall test above the 95% confidence level (Yue & Wang,
 182 2004).

183 Time averages are denoted by $\overline{\quad}$, while area-weighted averages are denoted using
 184 $\langle \quad \rangle$, where the area-weighted average of a function f is:

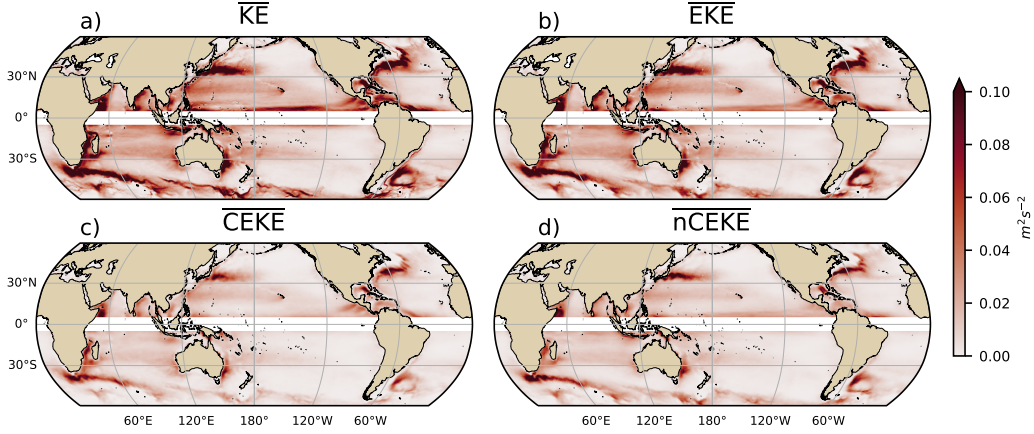
$$\langle f \rangle = \frac{\int f \xi dx dy}{\int \xi dx dy}, \quad (3)$$

185 where ξ is a mask that is set to zero in grid cells where no coherent eddies were iden-
 186 tified and one elsewhere.

187 3 Global Coherent Eddy Energetics

188 The kinetic energy decomposition estimated from sea surface height measured by
 189 satellite altimeters averaged from 1993-2019 is shown in Figure 2. These maps show that
 190 many regions of the global ocean are highly energetic in mean KE (\overline{KE}), mean EKE (\overline{EKE}),
 191 mean coherent eddy kinetic energy (\overline{CEKE}) and mean non-coherent eddy kinetic energy
 192 (\overline{nCEKE}). The spatial pattern highlights well-known regions of the ocean where mesoscale
 193 processes are abundant, such as the western boundary current (WBC) extensions and
 194 the Antarctic Circumpolar Current. The spatial distribution of the energy contained by
 195 the reconstructed mesoscale coherent eddies and non-coherent components are similar
 196 (Figures 2c,d). However, there are some regions where coherent eddies dominate over
 197 non-coherent, and vice-versa. Overall, this decomposition suggests that boundary cur-
 198 rent extensions and other energetic regions of the ocean contain both coherent and non-
 199 coherent components of the kinetic energy.

212 Eddy kinetic energy is known to be more than an order of magnitude greater than
 213 kinetic energy of the mean flow (MKE; Gill et al., 1974); this result is clearly shown in
 214 Figure 3a, which indicates that \overline{EKE} is responsible for almost all the \overline{KE} across the ocean,
 215 except for regions with persistent currents over time. Such regions are located in the mean
 216 boundary extension locations, the equatorial Pacific currents and regions in the Antarc-
 217 tic Circumpolar Current, where the \overline{EKE} explains around 40% of the \overline{KE} . In a previ-

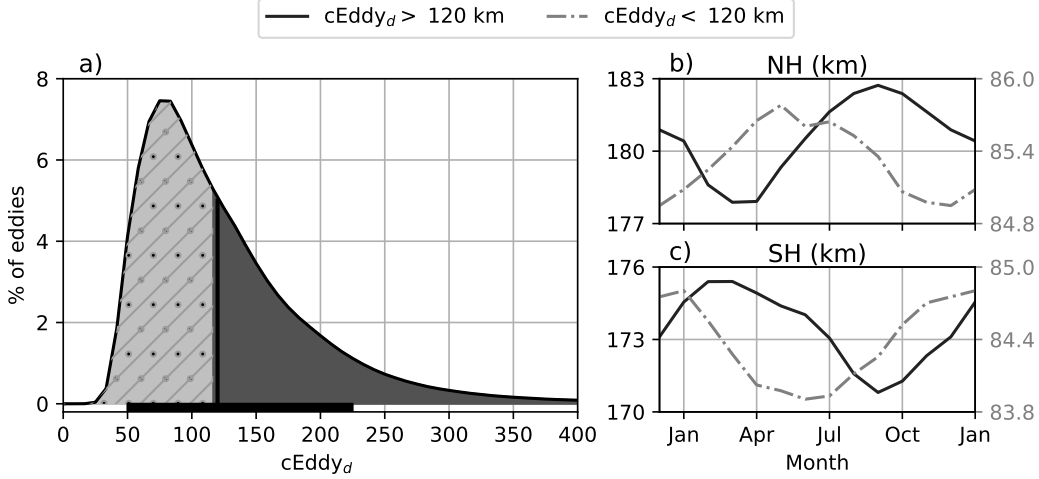


200 **Figure 2.** a) Mean surface kinetic energy (\overline{KE}); b) surface eddy kinetic energy (\overline{EKE}); c)
 201 surface coherent eddy kinetic energy (\overline{CEKE}), and d) surface non-coherent eddy kinetic energy
 202 (\overline{nCEKE}) averaged between 1993-2018.

218 our study, Chelton et al. (2011) estimated that the EKE within coherent eddies with life-
 219 times greater than 4 weeks contain between 40-60% of the \overline{EKE} . Our method to recon-
 220 struct the coherent eddy signature (Figure 3b) further corroborates that the coherent
 221 eddy component ($\langle \overline{CEKE} \rangle$) has $\sim 48\%$ of the $\langle \overline{KE} \rangle$ (Figure 3d). Furthermore, global area
 222 averages of the ratios show that $\langle \overline{EKE} \rangle$ explains $\sim 78\%$ of the ocean $\langle \overline{KE} \rangle$ field, while
 223 non coherent eddy features contain $\sim 57\%$ percent of the $\langle \overline{EKE} \rangle$. Note that the globally
 224 averaged coherent and non coherent components do not add to 100% as the cross terms
 225 (\mathcal{O}_c^2) are non-zero. The spatial pattern reveals a dominance of the \overline{CEKE} equatorward
 226 from the boundary current extensions and in areas with large coherent eddy contribu-
 227 tions of around 80% of the region's eddy kinetic energy, such as south of Australia, in
 228 the Tehuantepec Gulf, and in the tropical Atlantic. An evident signal is a reduction of
 229 the energy contained by coherent eddies at high latitudes and an increase in the energy
 230 explained by non-coherent eddies; this signal could be a consequence of the inability of
 231 the 0.25° satellite resolution (~ 13 km at 60° latitude) to resolve coherent eddies with
 232 scales smaller than ~ 10 km (first baroclinic Rossby radius at 60° ; Chelton et al., 1998).

233 Figure 4 shows the seasonal cycle of the area-weighted EKE and CEKE for the North-
 234 ern Hemisphere ($\langle EKE \rangle_{NH}$ and $\langle CEKE \rangle_{NH}$; $10^\circ N - 60^\circ N$) and Southern Hemisphere
 235 ($\langle EKE \rangle_{SH}$ and $\langle CEKE \rangle_{SH}$; $60^\circ S - 10^\circ S$). In both hemispheres, the $\langle EKE \rangle$ and $\langle CEKE \rangle$
 236 peak during summer. In the Northern Hemisphere, the largest $\langle EKE \rangle_{NH}$ and $\langle CEKE \rangle_{NH}$

203 Figure 3. Ratios of the kinetic energy components. a) Map of the proportion of mean eddy
204 kinetic energy (\overline{EKE}) versus mean kinetic energy (\overline{KE}); b) Map of the fraction of mean coherent
205 eddy kinetic energy (\overline{CEKE}) versus mean eddy kinetic energy (\overline{EKE}); c) Map of the fraction of
206 mean non-coherent eddy kinetic energy (\overline{nCEKE}) versus mean eddy kinetic energy (\overline{EKE}); d)
207 Global time and area averaged (represented by h i) fraction of mean eddy kinetic energy (\overline{EKE})
208 versus the global mean kinetic energy (\overline{KE}), area averaged fraction of mean coherent eddy
209 kinetic energy (\overline{CEKE}) and mean non coherent eddy kinetic energy (\overline{nCEKE}) versus global
210 mean eddy kinetic energy (\overline{EKE}). Regions where the depth of the ocean is shallower than
211 1000m are removed from the ratio estimation.

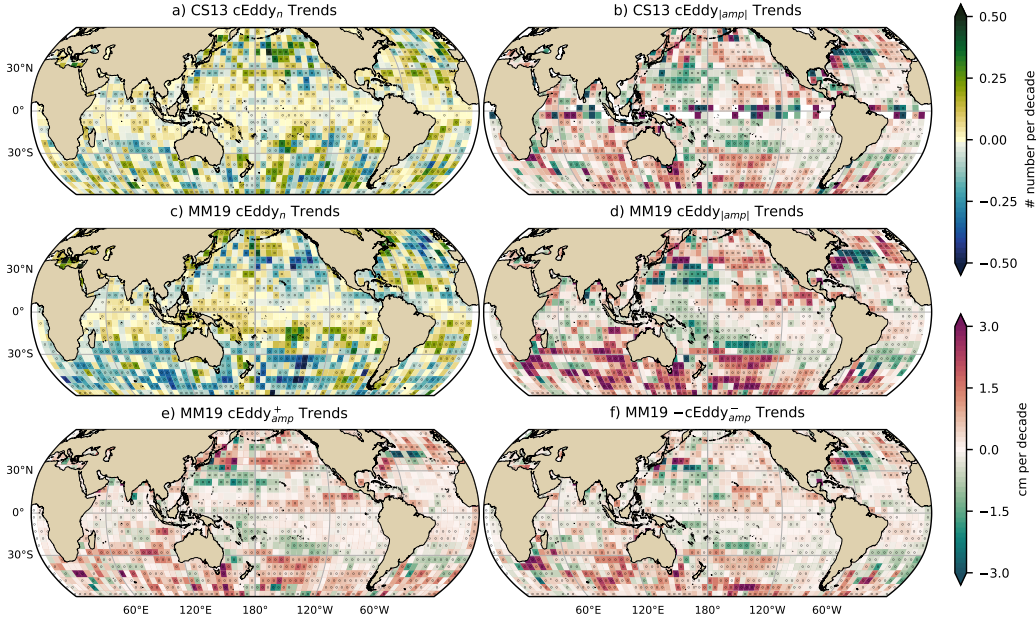


346 **Figure 7.** Distribution of the identified eddy diameter ($cEddy_d$; km) and hemispherical
 347 seasonality of the coherent eddy diameter. a) Distribution in percentage of identified eddy am-
 348 plitude, solid bar below distribution represents 90% of the identified eddies. Seasonal cycle of
 349 the eddy diameter for the b) Northern Hemisphere and c) Southern Hemisphere. Dark solid line
 350 and area corresponds to coherent eddies with diameters larger than 120 km, while light gray
 351 dash-dotted line and area shows coherent eddies with diameters smaller than 120 km.

363 5 Trends

364 The results presented in Figures 4 and 6 suggest a long-term readjustment of the
 365 coherent eddy field. The long-term trends of the number of coherent eddies, absolute co-
 366 herent eddy amplitude, and coherent eddy amplitude polarities are further explored in
 367 Figure 8 contrasting the MM19 and CS13 methods. Both MM19 and CS13 datasets show
 368 consistent spatial patterns in the trends and significance of the number of coherent ed-
 369 dies and the absolute coherent eddy amplitude. Several regions in the ocean, such as the
 370 Southern Ocean, North Atlantic and North Pacific, show a decrease in the number of ed-
 371 dies. Those same regions also have a clear increase in the absolute coherent eddy am-
 372 plitude. These trends are similar to those observed in mesoscale eddy kinetic energy (Martínez-
 373 Moreno et al., 2021) and provide additional evidence of a readjustment of the mesoscale
 374 eddy field over the last 3 decades.

375 The observed trends of $cEddy_{|amp|}$ in several oceanic regions have the same scale
 376 as sea level rise (~ 3 cm per decade). By analyzing the positive and negative coherent eddy
 377 amplitude, we filter out the observed trends that come from a net increase in sea level.



385 **Figure 8.** Trends of coherent eddy statistics. a) and b) Trends of the number of identified
 386 coherent eddies from satellite observations identified using the TrackEddy scheme of MM19,
 387 and those reported in CS13’s dataset. c) and d) Trends of the absolute value of identified coher-
 388 ent eddy amplitude ($cEddy_{|amp|}$) from satellite observations identified using TrackEddy (after
 389 MM19), and those reported by CS13. e) and f) Trends of the eddy amplitude polarity using
 390 TrackEddy ($cEddy_{amp}^+$ and $cEddy_{amp}^-$). Gray stippling shows regions that are statistically signifi-
 391 cant above the 95% confidence level.

378 In fact, each coherent eddy polarity has intensified in the Southern Ocean and North East
 379 Pacific and Atlantic. In other words, the amplitude of each polarity has increased over
 380 time, and thus this strengthening is an intrinsic response of the coherent eddy field. Note
 381 that the negative coherent eddy amplitude dominates the global $|cEddy_{amp}|$ trends (Fig-
 382 ure 8e, f). However, different trend patterns can be observed in both positive and neg-
 383 ative coherent eddy amplitudes in the North Atlantic and North Pacific, where the neg-
 384 ative coherent eddy amplitude in the Western Boundary Currents appears to decrease.

392 6 Regional Climatology

393 For regions with relatively large proportions of CEKE located at WBC extensions
 394 and eastern boundary currents, we investigate the seasonal and long-term variability of
 395 the coherent eddy properties. The most energetic WBC include the Gulf Stream, the Kuroshio

396 Current, and the Agulhas Current (Figures 9, 10, and 11). Coherent eddy generation in
 397 boundary current extensions occurs through baroclinic and barotropic instabilities of the
 398 mean current, thus all these regions share similar generation dynamics. In all these re-
 399 gions without exception; (i) CEKE contains 50-80% of the EKE in regions equatorward
 400 from the mean WBC extensions, (ii) the number of eddies is consistently small over the
 401 mean WBC extensions, and (iii) the eddy amplitude is larger over the mean WBC ex-
 402 tensions.

403 In the Gulf Stream, the energy ratio between CEKE and EKE is $\sim 56\%$ (Figure 9).
 404 The highest energy ratio occurs in regions with numerous eddies, colocated with regions
 405 where the largest $|\text{cEddy}_{amp}|$ gradients occur. The time series of cEddy_n and $\langle |\text{cEddy}_{amp}| \rangle$
 406 are anti-correlated (-0.52), and they display interannual and seasonal variability. Although
 407 Chaudhuri et al. (2009) observed that a positive phase of the North Atlantic Oscillation
 408 (NAO) exhibits higher EKE, due to an increase in baroclinic instability, thus suggest-
 409 ing more coherent eddies, we do not find a correlation between the cEddy_n or the $\langle |\text{cEddy}_{amp}| \rangle$
 410 in the Gulf Stream and the NAO index. Similar to the signal observed in the hemispheric
 411 analysis, the eddy count seasonal cycle follows the wind maximum lagging by ~ 3 months,
 412 while the amplitude of the coherent eddies lags by ~ 6 months.

421 The variability of the cEddy_n and $\langle |\text{cEddy}_{amp}| \rangle$ in the Kuroshio Current are weakly
 422 anti-correlated (-0.41; Figure 10). However, on average 56% of the energy in the region
 423 corresponds to CEKE. As observed in the Gulf Stream, there is an important seasonal
 424 cycle in the boundary extension, where the eddy count seasonal cycle occurs in March,
 425 lagging the wind maximum by ~ 3 months (January). Meanwhile, the amplitude of the
 426 coherent eddies lags the wind maximum by ~ 6 months (June).

433 In the Southern Hemisphere the strongest boundary current, the Agulhas Current,
 434 shows similar behavior to its counterparts in the Northern Hemisphere (Figure 11). On
 435 average, coherent eddies in the Agulhas Current contain $\sim 56\%$ of the energy, meanwhile
 436 the cEddy_n seasonal peak occurs in August, while the $\langle |\text{cEddy}_{amp}| \rangle$ peak occurs in January-
 437 February. The seasonal lag between the winds, eddy count, and eddy amplitude in each
 438 of the WBC extensions is interpreted as being analogous to the lagged response of co-
 439 herent eddy properties (Figure 6) due to eddy-eddy interactions, consistent with the in-
 440 verse cascade of energy.

413 Figure 9. Climatology of the eddy field and coherent eddy field in the Gulf Stream. a) Ratio
414 of mean coherent eddy kinetic energy ($\overline{\text{CEKE}}$) versus mean eddy kinetic energy ($\overline{\text{EKE}}$); b) Thick
415 lines show the running average over 2 years and thin lines show the running average over 90 days
416 of the coherent eddy number sum and the average coherent eddy amplitude; c) Map of the num-
417 ber of eddies; d) Map of the average coherent eddy amplitude; e) Seasonal cycle of the number
418 of eddies (cEddy_n); f) Seasonal cycle of the positive coherent eddy amplitude ($\text{cEddy}_{\text{amp}}^+$),
419 and g) Seasonal cycle of the negative coherent eddy amplitude ($\text{cEddy}_{\text{amp}}^-$). Contours in maps
420 correspond to mean sea surface height (m).

520 al., 2020; Wunsch, 2020; Martínez-Moreno et al., 2021). This long-term readjustment re-
521 veals an intensification of the coherent eddy field, possibly due to long-term readjust-
522 ments in the ocean baroclinic and barotropic instabilities, as well as the strength of the
523 winds.

524 The reconstruction of the coherent eddies and their statistics has revealed regions
525 with important coherent eddy contributions and a distinct seasonal evolution of the co-
526 herent eddies. Western boundary current (WBC) extensions generate eddies through the
527 instability of the main currents and the seasonal cycle of coherent eddies, CEKE, and
528 thus EKE could be associated with an inverse energy cascade observable through lagged
529 seasonal cycles in the coherent eddy statistics. In addition, the amplitude of the seasonal
530 cycle in WBC extensions is two times larger than any other region, thus the seasonal-
531 ity of the coherent eddies in WBC extensions dominates the hemispheric seasonal cy-
532 cle. Furthermore, the seasonal lag of the inverse energy cascade is coupled with the pres-
533 ence of fronts (Qiu et al., 2014), such as the case for WBC extensions, and our results
534 are consistent with the notion of baroclinic instability generating eddies and, via eddy-
535 eddy interactions, a lagged inverse energy cascade.

536 The use of satellite observations in this study limits our ability to quantify the im-
537 portance of the inverse energy cascade seasonality in the control of the coherent eddy
538 seasonal cycle. As mentioned above, there is robust evidence of an increase in eddy-eddy
539 interactions, however we cannot discard important contributions from other processes
540 such as the seasonal cycle of forcing, stratification, and instabilities, which are crucial
541 in the generation of coherent eddies. Although this study can provide a descriptive re-
542 sponse of the coherent eddy field, further work is needed to assess the role of eddy-eddy
543 interactions in our changing climate, ocean dynamics, and biogeochemical processes. Fur-
544 thermore, the SWOT mission could allow us to advance our understanding of eddy-eddy
545 interactions and the seasonal cycle of scales smaller than mesoscale, which may provide
546 further evidence of the inverse energy cascade driving the coherent eddy seasonality. Cur-
547 rent generation climate models have just started to resolve mesoscale dynamics, thus,
548 the presented estimate of energy in coherent eddies from satellite observations could be
549 used as a benchmark that facilitates the evaluation of such models, and to quantify the
550 energy contained by mesoscale and more specifically coherent eddies in future climate
551 projections.

Acknowledgments

The Chelton & Schlax (2013) dataset was produced by SSALTO/DUACS and distributed by AVISO+ (<https://www.avis0.altimetry.fr/>) with support from CNES, developed and validated in collaboration with E.Mason at IMEDEA. Global coherent eddy reconstruction, coherent and non-coherent eddy kinetic energy datasets, in addition to gridded coherent eddy tracking datasets are publicly available at (<https://doi.org/10.5281/zenodo.4646429>). All analyses and figures in this manuscript are reproducible via Jupyter notebooks and instructions can be found in the Github repository `CEKE.climatology` (<https://github.com/josuemtzmo/CEKE.climatology>). Trends used the Python Package `xarrayMannKendall` (<https://doi.org/10.5281/zenodo.4458776>). J.M.-M. was supported by the Consejo Nacional de Ciencia y Tecnología (CONACYT), Mexico funding. M.H.E. is supported by the Centre for Southern Hemisphere Oceans Research (CSHOR), a joint research centre between Qingdao National Laboratory for Marine Science and Technology (QNLN), Commonwealth Scientific and Industrial Research Organisation (CSIRO), University of New South Wales (UNSW), and the University of Tasmania (UTAS). Analyses were undertaken on the National Computational Infrastructure in Canberra, Australia, which is supported by the Australian Commonwealth Government.

References

- Arbic, B. K., Polzin, K. L., Scott, R. B., Richman, J. G., & Shriver, J. F. (2013). On Eddy Viscosity, Energy Cascades, and the Horizontal Resolution of Gridded Satellite Altimeter Products*. *Journal of Physical Oceanography*, *43*(2), 283–300. doi: 10.1175/jpo-d-11-0240.1
- Ashkezari, M. D., Hill, C. N., Follett, C. N., Forget, G., & Follows, M. J. (2016). Oceanic eddy detection and lifetime forecast using machine learning methods. *Geophysical Research Letters*, *43*(23). doi: 10.1002/2016gl071269
- Beron-Vera, F. J., Wang, Y., Olascoaga, M. J., Goni, G. J., & Haller, G. (2013). Objective Detection of Oceanic Eddies and the Agulhas Leakage. *Journal of Physical Oceanography*, *43*(7), 1426–1438. doi: 10.1175/JPO-D-12-0171.1
- Bouali, M., Sato, O. T., & Polito, P. S. (2017). Temporal trends in sea surface temperature gradients in the South Atlantic Ocean. *Remote Sensing of Environment*, *194*, 100–114. doi: 10.1016/j.rse.2017.03.008
- Callies, J., Flierl, G., Ferrari, R., & Fox-Kemper, B. (2015). The role of mixed-layer

- 584 instabilities in submesoscale turbulence. *Journal of Fluid Mechanics*, 788, 5–41.
 585 doi: 10.1017/jfm.2015.700
- 586 Cane, M. A., Clement, A. C., Kaplan, A., Kushnir, Y., Pozdnyakov, D., Seager, R.,
 587 ... Murtugudde, R. (1997). Twentieth-Century Sea Surface Temperature Trends.
 588 *Science*, 275(5302), 957–960. doi: 10.1126/science.275.5302.957
- 589 Chaudhuri, A. H., Gangopadhyay, A., & Bisagni, J. J. (2009). Interannual variabil-
 590 ity of Gulf Stream warm-core rings in response to the North Atlantic Oscillation.
 591 *Continental Shelf Research*, 29(7), 856–869. doi: 10.1016/j.csr.2009.01.008
- 592 Chelton, D. B., A, d. R., Schlax, M. G., Naggar, K., & Siwertz, N. (1998). Geo-
 593 graphical variability of the first baroclinic Rossby radius of deformation. *Journal*
 594 *of Physical Oceanography*, 28(3), 433–460. doi: 10.1175/1520-0485(1998)028<0433:
 595 GVOTFB>2.0.CO;2
- 596 Chelton, D. B., Gaube, P., Schlax, M. G., Early, J. J., & Samelson, R. M. (2011).
 597 The influence of nonlinear mesoscale eddies on near-surface oceanic chlorophyll.
 598 *Science*, 334(6054), 328–32. doi: 10.1126/science.1208897
- 599 Chelton, D. B., & Schlax, M. G. (2013). *Mesoscale eddies in altimeter observations*
 600 *of ssh*.
- 601 Chelton, D. B., Schlax, M. G., Samelson, R. M., & de Szoeke, R. A. (2007). Global
 602 observations of large oceanic eddies. *Geophysical Research Letters*, 34(15),
 603 L15606. doi: 10.1029/2007GL030812
- 604 CMEMS. (2017). The Ssalto/Duacs altimeter products were produced and dis-
 605 tributed by the Copernicus Marine and Environment Monitoring Service. *Aviso*
 606 *Dataset*. Retrieved from <https://www.aviso.altimetry.fr/>
- 607 Cui, W., Wang, W., Zhang, J., & Yang, J. (2020). Identification and census statis-
 608 tics of multicore eddies based on sea surface height data in global oceans. *Acta*
 609 *Oceanologica Sinica*, 39(1), 41–51. doi: 10.1007/s13131-019-1519-y
- 610 Faghmous, J. H., Frenger, I., Yao, Y., Warmka, R., Lindell, A., & Kumar, V. (2015,
 611 6). A daily global mesoscale ocean eddy dataset from satellite altimetry. *Scientific*
 612 *Data*, 2, 150028 EP -. doi: 10.1038/sdata.2015.28
- 613 Ferrari, R., & Wunsch, C. (2009). Ocean Circulation Kinetic Energy: Reservoirs,
 614 Sources, and Sinks. *Annual Review of Fluid Mechanics*, 41(1), 253–282. doi: 10
 615 .1146/annurev.fluid.40.111406.102139
- 616 Frenger, I., Gruber, N., Knutti, R., & Münnich, M. (2013). Imprint of Southern

- 617 Ocean eddies on winds, clouds and rainfall. *Nature Geoscience*, 6(8), 608 EP -.
618 doi: 10.1038/ngeo1863
- 619 Frenger, I., Münnich, M., Gruber, N., & Knutti, R. (2015). Southern Ocean eddy
620 phenomenology. *Journal of Geophysical Research: Oceans*, 120(11), 7413-7449.
621 doi: 10.1002/2015JC011047
- 622 Fu, L., Chelton, D., Le Traon, P., & Oceanography, M. R. (2010). Eddy dynamics
623 from satellite altimetry. *Oceanography*, 23(4), 14-25. doi: 10.2307/24860859
- 624 Gill, A., Green, J., & Simmons, A. (1974). Energy partition in the large-scale ocean
625 circulation and the production of mid-ocean eddies. *Deep Sea Res Oceanogr Abstr*,
626 21(7), 499-528. doi: 10.1016/0011-7471(74)90010-2
- 627 Hogg, A. M., & Blundell, J. R. (2006). Interdecadal variability of the southern
628 ocean. *Journal of Physical Oceanography*, 36(8), 1626-1645. doi: 10.1175/
629 JPO2934.1
- 630 Hogg, A. M., Meredith, M. P., Chambers, D. P., Abrahamsen, E. P., Hughes,
631 C. W., & Morrison, A. K. (2015). Recent trends in the Southern Ocean
632 eddy field. *Journal of Geophysical Research: Oceans*, 120(1), 257-267. doi:
633 10.1002/2014JC010470
- 634 Hu, S., Sprintall, J., Guan, C., McPhaden, M. J., Wang, F., Hu, D., & Cai,
635 W. (2020, 2). Deep-reaching acceleration of global mean ocean circula-
636 tion over the past two decades. *Science Advances*, 6(6), eaax7727. doi:
637 10.1126/sciadv.aax7727
- 638 Japan Meteorological Agency, Japan. (2013). *Jra-55: Japanese 55-year reanalysis,*
639 *daily 3-hourly and 6-hourly data.* Boulder CO: Research Data Archive at the Na-
640 tional Center for Atmospheric Research, Computational and Information Systems
641 Laboratory. Retrieved from <https://doi.org/10.5065/D6HH6H41>
- 642 Kang, D., & Curchitser, E. N. (2013). Gulf stream eddy characteristics in a high-
643 resolution ocean model. *Journal of Geophysical Research: Oceans*, 118(9), 4474-
644 4487. Retrieved from [https://agupubs.onlinelibrary.wiley.com/doi/abs/10](https://agupubs.onlinelibrary.wiley.com/doi/abs/10.1002/jgrc.20318)
645 [.1002/jgrc.20318](https://doi.org/10.1002/jgrc.20318) doi: <https://doi.org/10.1002/jgrc.20318>
- 646 Kang, D., & Curchitser, E. N. (2017). On the Evaluation of Seasonal Variability of
647 the Ocean Kinetic Energy. *Geophysical Research Letters*, 47, 1675-1583. doi: 10
648 [.1175/JPO-D-17-0063.1](https://doi.org/10.1175/JPO-D-17-0063.1)
- 649 Li, G., Cheng, L., Zhu, J., Trenberth, K. E., Mann, M. E., & Abraham, J. P. (2020).

- 650 Increasing ocean stratification over the past half-century. *Nature Climate Change*,
 651 1–8. doi: 10.1038/s41558-020-00918-2
- 652 Martínez-Moreno, J., Hogg, A. M., England, M., Constantinou, N. C., Kiss, A. E.,
 653 & Morrison, A. K. (2021). Global changes in oceanic mesoscale currents over the
 654 satellite altimetry record. *Journal of Advances in Modeling Earth Systems*, 0(ja).
 655 doi: 10.1029/2019MS001769
- 656 Martínez-Moreno, J., Hogg, A. M., Kiss, A. E., Constantinou, N. C., & Morrison,
 657 A. K. (2019). Kinetic energy of eddy-like features from sea surface altime-
 658 try. *Journal of Advances in Modeling Earth Systems*, 11(10), 3090-3105. doi:
 659 10.1029/2019MS001769
- 660 Patel, R. S., Llorc, J., Strutton, P. G., Phillips, H. E., Moreau, S., Pardo, P. C.,
 661 & Lenton, A. (2020). The Biogeochemical Structure of Southern Ocean
 662 Mesoscale Eddies. *Journal of Geophysical Research: Oceans*, 125(8). doi:
 663 10.1029/2020jc016115
- 664 Pilo, G. S., Mata, M. M., & Azevedo, J. L. L. (2015). Eddy surface properties and
 665 propagation at Southern Hemisphere western boundary current systems. *Ocean
 666 Science*, 11(4), 629–641. doi: 10.5194/os-11-629-2015
- 667 Qiu, B. (1999). Seasonal Eddy Field Modulation of the North Pacific Subtropical
 668 Countercurrent: TOPEX/Poseidon Observations and Theory. *Journal of Physical
 669 Oceanography*, 29(10), 2471–2486. doi: 10.1175/1520-0485(1999)029<2471:sefmot>2
 670 .0.co;2
- 671 Qiu, B., & Chen, S. (2004). Seasonal Modulations in the Eddy Field of the South
 672 Pacific Ocean. *Journal of Physical Oceanography*, 34(7), 1515–1527. doi: 10.1175/
 673 1520-0485(2004)034<1515:smitef>2.0.co;2
- 674 Qiu, B., Chen, S., Klein, P., Sasaki, H., & Sasai, Y. (2014). Seasonal Mesoscale
 675 and Submesoscale Eddy Variability along the North Pacific Subtropical Coun-
 676 tercurrent. *Journal of Physical Oceanography*, 44(12), 3079–3098. doi:
 677 10.1175/JPO-D-14-0071.1
- 678 Ruela, R., Sousa, M. C., deCastro, M., & Dias, J. M. (2020). Global and regional
 679 evolution of sea surface temperature under climate change. *Global and Planetary
 680 Change*, 190, 103190. doi: 10.1016/j.gloplacha.2020.103190
- 681 Sasaki, H., Klein, P., Qiu, B., & Sasai, Y. (2014). Impact of oceanic-scale inter-
 682 actions on the seasonal modulation of ocean dynamics by the atmosphere. *Nature*

- 683 *Communications*, 5(1), 5636. doi: 10.1038/ncomms6636
- 684 Schubert, R., Schwarzkopf, F. U., Baschek, B., & Biastoch, A. (2019). Submesoscale
685 Impacts on Mesoscale Agulhas Dynamics. *Journal of Advances in Modeling Earth*
686 *Systems*, 11(8), 2745–2767. doi: 10.1029/2019ms001724
- 687 Siegel, D., Peterson, P., DJ, M., Maritorena, S., & Nelson, N. (2011). Bio-optical
688 footprints created by mesoscale eddies in the Sargasso Sea. *Geophysical Research*
689 *Letters*, 38(13), n/a-n/a. doi: 10.1029/2011GL047660
- 690 Uchida, T., Abernathey, R., & Smith, S. (2017). Seasonality of eddy kinetic energy
691 in an eddy permitting global climate model. *Ocean Modelling*, 118, 41-58. doi: 10
692 .1016/j.ocemod.2017.08.006
- 693 Wunsch, C. (2020). Is The Ocean Speeding Up? Ocean Surface Energy Trends.
694 *Journal of Physical Oceanography*, 50(11), 1–45. doi: 10.1175/jpo-d-20-0082.1
- 695 Wunsch, C., & Ferrari, R. (2004). Vertical mixing, energy, and the general circula-
696 tion of the oceans. *Annual Review of Fluid Mechanics*, 36(1), 281–314. doi: 10
697 .1146/annurev.fluid.36.050802.122121
- 698 Wyrтки, K., Magaard, L., & Hager, J. (1976). Eddy energy in the oceans. *Journal of*
699 *Geophysical Research*, 81(15), 2641-2646. doi: 10.1029/JC081i015p02641
- 700 Yue, S., & Wang, C. (2004). The Mann-Kendall Test Modified by Effective Sample
701 Size to Detect Trend in Serially Correlated Hydrological Series. *Water Resources*
702 *Management*, 18(3), 201–218. doi: 10.1023/b:warm.0000043140.61082.60
- 703 Zamudio, L., Hurlburt, H. E., Metzger, E. J., Morey, S. L., O’Brien, J. J., Tilburg,
704 C., & Zavala-Hidalgo, J. (2006). Interannual variability of Tehuantepec ed-
705 dies. *Journal of Geophysical Research: Oceans (1978–2012)*, 111(C5). doi:
706 10.1029/2005JC003182